Delayed Transition to Coherent Emission in Nanolasers with Extended Gain Media

F. Lohof,[1,*] R. Barzel,[1] P. Gartner,[2] and C. Gies[1]

[1] *Institute for Theoretical Physics, University of Bremen Otto-Hahn-Allee 1, P.O. Box 330440, Bremen, Germany*

[2] *Centre International de Formation et de Recherche Avancées en Physique – National Institute of Materials Physics, P.O. Box MG-7, Bucharest-Măgurele, Romania*

(Received 10 August 2018; revised manuscript received 23 October 2018; published 26 November 2018)

The realization of high-β lasers is one of the prime applications of cavity QED promising ultralow thresholds, integrability, and reduced power consumption in the field of *green photonics*. In such nanolasers, spontaneous emission can play a central role even above the threshold. By going beyond rate-equation approaches, we revisit the definition of a laser threshold in terms of the input-output characteristics and the degree of coherence of the emission. We demonstrate that there are new regimes of cavity-QED lasing, realized, e.g., in high-Q nanolasers with extended gain material, for which the two can differ significantly such that coherence is reached at much higher pump powers than required to observe the thresholdlike intensity jump. Against the common perception, such devices do not benefit from high-β factors in terms of power reduction, as a significant amount of stimulated emission is required to quieten the spontaneous emission noise.

DOI: 10.1103/PhysRevApplied.10.054055

I. INTRODUCTION

Lasers have been around for almost 60 years and most of the underlying physics is well established and understood. The threshold, in particular, is the central defining property of any laser device, as it separates the regime of spontaneous emission from that of phase-coherent operation. In conventional laser devices, the threshold can easily be identified from the input-output characteristics alone: Below threshold, a majority of photons spontaneously emitted from the gain material is lost, and only a fraction described by the β factor ends up in the modes that can ultimately achieve lasing. Above threshold, stimulated emission into these modes completely overpowers the losses, which gives rise to an intensity jump typically over several orders of magnitude, which clearly marks the laser threshold ("intensity threshold"). This fundamental behavior can already be understood in terms of coupled rate equations for the excitation of the gain material and the photon number [1,2].

In recent times, the laser threshold has been revisited due to the uprise of nanolasers that operate in new cavity-enhanced lasing regimes [3–5]. *Nature Photonics* was amongst the first journals to issue a laser "checklist" to ensure a certain standard in identifying laser operation, which becomes even more important for small lasers [6]. Cavities with ultra-small mode volumes with dimensions of the light's wavelength allow for tinkering with spontaneous emission itself. Quantum-electrodynamical effects make it possible to enhance the emission rate [7,8], to suppress emission into nonlasing modes [9–11], or do both at the same time—thereby fundamentally changing the contributions from spontaneous and stimulated emission. When spontaneous emission is nearly completely directed into the laser mode ($\beta \approx 1$), the intensity jump even disappears and makes an identification of the threshold from the input-output curve alone impossible [12–14]. In such thresholdless lasers, it has become common practice to investigate fluctuations in the photon number n that are captured in the two-photon correlation function [3,15,16]

$$g^{(2)}(0) = \frac{\langle n^2 \rangle - \langle n \rangle}{\langle n \rangle^2}. \tag{1}$$

For coherent emission, $g^{(2)}(0)$ takes on the value of 1, whereas for spontaneously emitted light below threshold it has a fingerprint $g^{(2)}(0) = 2$. As we show, the increased role of spontaneous emission in nanolasers can substantially delay the formation of coherence to higher pump powers.

In the present work, we refine the definition of the laser threshold by going beyond the rate-equation approximation to take a combined look at the intensity threshold and the transition of the emission from thermal to coherent light reflected in $g^{(2)}(0)$ ("coherence threshold"). While one might intuitively believe that both characteristics are

*flohof@itp.uni-bremen.de

interlinked and one necessitates the other, we show that there are operational regimes of nanolasers that give rise to a separation between the two thresholds, so that the emission becomes coherent at much higher excitations, after the intensity threshold has been crossed. An important result of this finding is that one commonly used criterion for lasing in cavity-enhanced nanolasers, i.e., the mean intracavity photon number $n = 1$, can be arbitrarily insufficient and truly only holds in the limit of the single-emitter laser [8,17,18]. Furthermore, in those regimes an increase of the β factor has no benefit in terms of reducing the threshold power, an aspect that has, to the best of our knowledge, not been recognized in the literature so far. The implications are both of fundamental relevance for understanding the laser threshold, and apply to present-day nanolaser devices. Despite the simplicity of our model, it captures all relevant effects of the laser dynamics and allows for the definition of analytical expressions for the above-mentioned threshold criteria.

II. CHARACTERIZING THE LASER THRESHOLD BEYOND THE RATE-EQUATION APPROXIMATION

At the rate-equation level the laser threshold is defined in terms of the output intensity. This criterion we define as the intensity threshold. In conventional lasers it is well established that the threshold marking the transition to coherent emission is accompanied by a sharp increase of output intensity. This intensity jump is less pronounced or vanishes completely in high-β lasers. Here we consider N independent two-level emitters in resonant Jaynes-Cummings interaction with a single mode of an optical cavity [19]. This simplified laser model provides analytic access to quantities related to the threshold, yet it contains the relevant physics to render its implications applicable to current cavity-QED nanolaser devices. Starting from the system Hamiltonian we derive equations of motion for the upper-level population f (the lower-level population is $1-f$) and the intracavity photon number n that resemble standard laser rate equations [20] (see Appendix A):

$$\dot{f} = -R\,[n(2f-1)+f] - \gamma f + P(1-f), \tag{2a}$$

$$\dot{n} = RN\,[n(2f-1)+f] - \kappa n, \tag{2b}$$

where

$$R = \frac{4|g|^2}{P+\gamma+\kappa} \tag{3}$$

is the spontaneous emission rate in the cavity mode, g is the light-matter interaction strength, γ is the rate of radiative losses, P is the pump rate, and κ is the cavity decay rate. The β factor is defined as the ratio of the spontaneous emission into the laser mode R to the total spontaneous emission including losses, i.e.,

$$\beta = R/(R+\gamma). \tag{4}$$

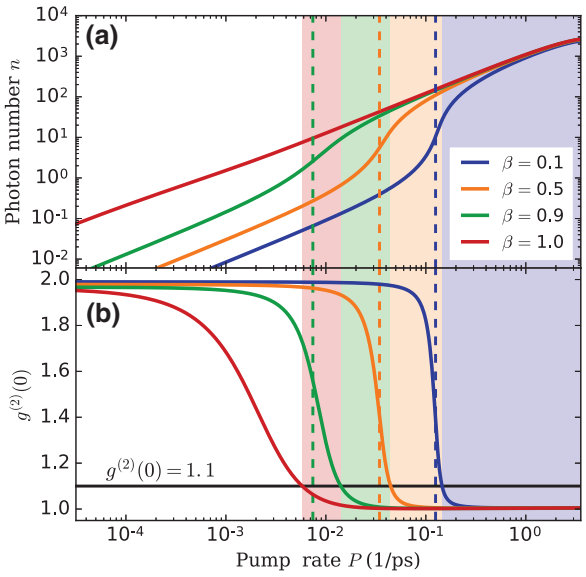

FIG. 1. (a) Output intensity and (b) $g^{(2)}(0)$ values according to Eqs. (2) and (6) are shown for different values of β. The parameters $N = 100$, $\kappa = 0.04$ ps^{-1}, and $g = 0.03$ ps^{-1} correspond to typical high-Q quantum dot nanolasers [16]. The intensity thresholds are marked as dashed lines. In this parameter regime, they nearly coincide with the threshold to coherent emission, which are indicated by the shaded regions for each value of β.

In their stationary limit, the rate equations can be used to define the pump value P_{th} of the intensity threshold. In Appendix A, we show that it obeys the equation

$$P_{\mathrm{th}} - \gamma - (P_{\mathrm{th}}+\gamma)\frac{\kappa}{RN} = 0. \tag{5}$$

The functionality of the threshold pump rate P_{th} defined this way is illustrated in the top panel of Fig. 1. For typical quantum-dot (QD) nanolaser parameters taken from [16], output intensities are shown (solid lines) together with the respective values for P_{th} marked by the vertical lines. Different values of β are used to characterize different device efficiencies as explained below. As can be seen, the threshold pump rates determined from Eq. (5) lie exactly in the middle of the corresponding jump intervals in the output intensities.

Due to excitation-induced dephasing, the emission rate R depends on the pump rate. With it, β is implicitly excitation dependent. Nevertheless, since a constant β factor is well established throughout the literature to characterize laser efficiency, we choose to use β rather than the emission rate γ into nonlasing modes, which is more commonly used in theory. To do so, all given values of β are evaluated at $P = P_{\mathrm{th}}$. While nonconstant β factors have been

investigated in different contexts [21–23], this approximate treatment fully serves the purpose in this work.

For β approaching unity, the intensity jump goes to zero, reflecting the concept of thresholdless lasing often referred to in the literature [12–14]. However, it is well established that coherent emission can take place at finite excitation even in the limiting case $\beta = 1$ [24]. With no distinct threshold nonlinearity in the output intensity of high-β lasers, one has to rely on *statistical* properties of the emission in order to identify lasing [3,15,16]. In a classical picture, the output intensity fluctuates around its mean value, which allows distinguishing a thermal from a coherent light source. The laser model we employ is fully quantum mechanical. In this picture, a coherent (thermal) state of the light field is characterized by a Poissonian (Bose-Einstein) photon distribution function p_n. This quantity can be accessed both in theory by using master-equation approaches [25–28], and in experiment by using photon-number-resolved detection schemes [29,30]. In practice, it is much easier to use the second-order photon autocorrelation function $g^{(2)}(0)$ to characterize the emission, as it can be readily measured using Hanbury Brown and Twiss setups [31]. It is defined in Eq. (1), with $\langle n^k \rangle = \sum_n p_n n^k$, and the transition to its coherent value of 1 has become an established method to characterize nanolasers that operate close to the thresholdless regime with $\beta \approx 1$ [3,15,16].

We access the two-photon correlation function beyond the rate-equation limit by extending Eqs. (2) to contain higher-order correlations and truncate the arising hierarchy of quantum-mechanical expectation values up to and including two-photon correlations [24]. This approach, the details of which are given in Appendix B, allows us to arrive at an analytic expression for the photon autocorrelation function that only contains the photon number n, the carrier occupation f, and fixed system parameters

$$g^{(2)}(0) = 2 - \frac{\frac{R}{n}(2n+1)(n+f) + \frac{2\kappa}{N}}{\kappa + \frac{\Gamma}{2} + R(2n+1) - \frac{R\Gamma}{2\kappa}N(2f-1)}, \quad (6)$$

where we define $\Gamma = P + \gamma + \kappa$. By using the stationary values for f and n provided by the rate equations and taking advantage of the relationship between them

$$f = n\frac{NR+\kappa}{NR(2n+1)}, \quad (7)$$

which follows from Eq. (2b) in steady state, Eq. (6) can be further simplified to obtain a closed analytic expression for $g^{(2)}(0)$ in terms of the photon number only:

$$g^{(2)}(0) = 2 - \frac{R(2n+2) + \frac{3\kappa}{N}}{R(2n+1) + \kappa + \frac{\Gamma}{2\kappa}\frac{NR+\kappa}{2n+1}}. \quad (8)$$

This expression is a key result of the paper, it provides access to the statistical properties of the emission even when values for the photon number obtained from rate equations are inserted. In Appendix B we show that the results obtained from Eq. (8) agree extremely well with the full solution from the extended quadruplet equations so that, in fact, it can be used to augment results of rate-equation calculations with the corresponding $g^{(2)}(0)$ values.

In Fig. 1, the photon correlation function $g^{(2)}(0)$ as obtained from Eq. (6) is shown together with output intensities for different β factors. At low excitations $g^{(2)}(0)$ exhibits a value of 2. As it is customary in the literature, we model the excitation as an incoherent process, described by a Lindblad term [see Eq. (A2)]. It represents physically the scenario where intermediate scattering processes from higher excited ones to the final states before recombination dephase any phase information that may have been imprinted by the exciting laser. As a result, the emitted photons exhibit no phase coherence leading to thermal emission with $g^{(2)}(0) = 2$. For all values of β, the transition of $g^{(2)}(0)$ to 1 (marked by the shaded regions) indicating coherent emission closely follows the intensity threshold (marked by the vertical lines). This behavior corresponds to the common conception of the intensity threshold being interlinked with the transition to coherent emission. Only for $\beta = 1$ the intensity threshold vanishes and solely $g^{(2)}(0)$ indicates the existence of a transition.

We define the coherence threshold P_{coh} as the point, where $g^{(2)}(0)$ indicates the onset of coherent emission. Here we choose $g^{(2)}(0) = 1.1$ with the aim to identify the beginning of an interval in which $g^{(2)}(0)$ stays practically constant around unity. Of course, the choice of 1.1 for $g^{(2)}(0)$ as the onset of coherence is to a certain extent arbitrary, however, a lower value would only push the coherence and the intensity thresholds even further from one another. It is important to point out that a unique definition of P_{coh} is only possible in the limit $\beta \to 0$. For large values of β that are relevant in nanolasers, $g^{(2)}(0)$ approaches 1 gradually over a wide range of excitation powers.

III. NEW LASER REGIMES

We now turn to a different class of nanolasers and show that they elude the common conception of the laser threshold. Until now, high-Q nanolasers were mostly realized in high-Q cavities with discrete emitters, such as quantum dots, as gain material. The previous section illustrated that for these systems, the formation of coherence is linked to the intensity threshold as one typically expects. A fundamentally different behavior is encountered in a very different, yet highly relevant regime of cavity-QED nanolasers that operate with extended gain materials instead of individual emitters. Atomically thin layers of semiconducting transition-metal dichalcogenides (TMDs), such as WSe_2

or MoS_2, have recently moved into the focus of optoelectronic device applications [32] including nanolasers [33–36]. These new materials combine advantages in ease of fabrication over conventional III/V semiconductors with a plethora of possibilities to engineer their electronic and optical properties. The possibility of population inversion [37] and room-temperature lasing with monolayer TMD flakes on top of photonic crystal [36] or nanobeam [33] cavities is being vividly discussed in the literature. Also recently, room-temperature lasing from a two-dimensional GaN quantum well (QW) embedded in a nanobeam cavity has been demonstrated [26].

Typical carrier densities in extended gain media (of the order of 10^{13} cm^{-2} in two-dimensional TMD materials) strongly exceed carrier numbers in discrete gain media, such as quantum dots. This results in very different operational regimes with severe implications regarding the threshold behavior. While more complex semiconductor laser models can be employed [26,38,39], for the present purpose it suffices to bear with the formalism used up to this point by mapping the number of electron-hole pairs in the two-dimensional gain media to our discrete-emitter model. This notion is formally justified, since the creation of cavity photons results from the recombination of an electron-hole pair both in the case of N independent emitters each containing a single excitation, or N excitations in an extended system. Assuming an active region of 0.3 μm^2 and a typical carrier density of 10^{13} cm^{-2} yields an estimate for the maximum number of excitons of $N = 3 \times 10^4$. The parameters we use in the following correspond to that of the nanobeam-quantum-well laser investigated by Jagsch *et al.* [26]. In addition to much larger N, reported Q factors for both the nanobeam and TMD nanolasers are significantly lower and are typically around 2500 [26,33–36].

Input-output curves and photon-autocorrelation functions corresponding to the parameters of Ref. [26], but also applicable to recent work on TMD gain media, are shown in Fig. 2. As for the few-emitter case (Fig. 1), the intensity threshold, marked by the intensity jump in the input-output curves, moves to lower pump rates with increasing β factor, suggesting that the threshold current can be strongly reduced by maximizing the β factor. The corresponding autocorrelation functions are shown in the lower panel and reveal a very different picture: The transition to coherent emission is strongly offset to higher pump rates from the intensity jump, so that, in fact, the coherence and intensity thresholds are no longer aligned. Coherent emission is reached at a pump rate of about 0.07/ps *irrespective* of the value of β, implying that for devices with extended gain media, a reduction of the threshold current is no longer possible by reducing radiative losses (i.e., increasing β).

This behavior, which is a key insight of this work, can be attributed to the very distinct parameter regimes: Room-temperature lasing from the extended gain media in

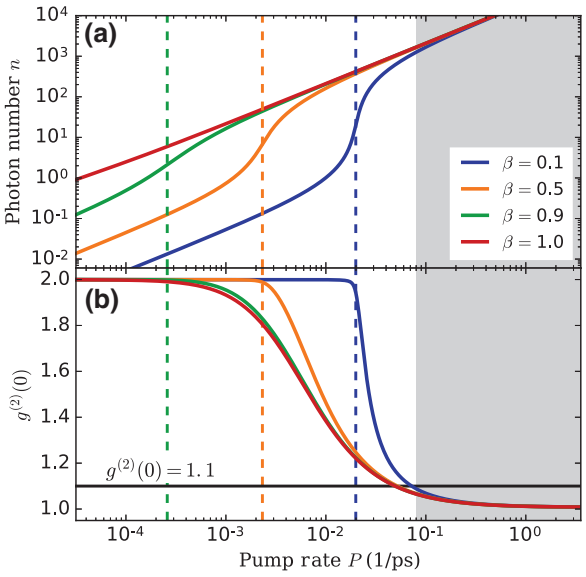

FIG. 2. For a nanolaser with an extended gain material, (a) output intensity and (b) $g^{(2)}(0)$ values are shown for different β. The large carrier number in the gain media is reflected in $N = 3 \times 10^4$, whereas the other parameters are $\kappa = 0.7$ ps^{-1}, $g = 0.02$ ps^{-1}. For all values of β, the intensity threshold (dashed vertical lines) is clearly separated from the transition to coherent emission (indicated by the gray area). Furthermore, the coherence thresholds indicate that increasing β has no benefit in terms of reducing the pump power to reach coherent emission.

Refs. [26] and [33] takes place in a regime, where cavity losses are the dominant quantity in determining the laser threshold. Despite the relatively low Q factors, lasing is still possible due to the large number of carriers producing gain. For few-emitter nanolasers, as the systems summarized in Ref. [8], a much larger cavity Q is required to attain lasing, which sets an upper bound for κ. In this low-κ regime, radiative losses dominate over the cavity losses, so that the threshold pump rate is strongly dependent on β. These results are summarized in Fig. 3, which compares the pump rate P_{coh}, at which coherent emission is reached, for the few-emitter (dashed lines) and extended gain media (solid lines) as a function of the cavity loss rate. The cavity loss rates for both operational regimes we consider are indicated by vertical lines.

More insight is revealed by condensing the information in Fig. 2 into a depiction of $g^{(2)}(0)$ as a function of the mean photon number. Surprisingly, for the parameters of the extended gain media (solid lines), Fig. 4 shows that the transition to coherent emission is solely determined by the mean intracavity photon number completely irrespective of the value of β. Coherence is reached at $n \approx 1000$, which greatly exceeds the $n = 1$ criterion that has frequently been used to indicate the threshold [3,40,41]. To emphasize the contrasting behavior to the few-emitter nanolaser, the results of Fig. 1 are shown as dashed lines. Here, coherence

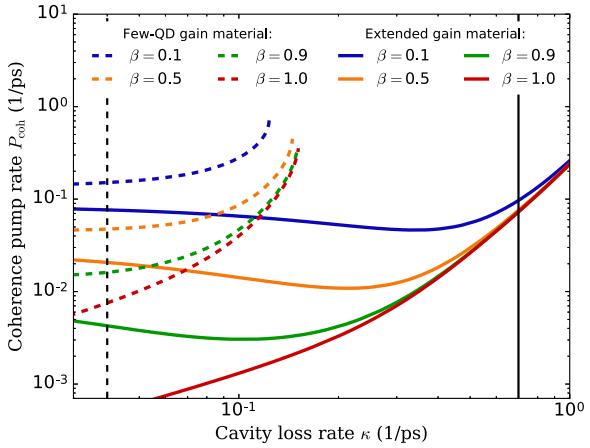

FIG. 3. Pump rate P_{coh} at the coherence threshold as a function of cavity loss rate κ. Parameters (N, g) correspond to those in Figs. 1 (dashed) and 2 (solid). Vertical lines indicate respective values for κ. One observes the different dependence on β for the two cases as well as the transition between the regimes for varying κ. For a small number of emitters there is an upper bound for κ beyond which lasing can not be achieved and thus the dashed lines terminate above a certain value.

is reached at significantly lower mean photon numbers ($n \approx 10$ for $\beta \to 1$), and one observes a clear reduction in the photon number necessary to reach coherence by increasing β. The consequences of this finding are highly relevant for the design of future nanolasers that aim to exploit the unique properties of two-dimensional TMD and QW gain materials: Here, a reduction in energy consumption requires improving the cavity Q instead of minimizing radiative losses.

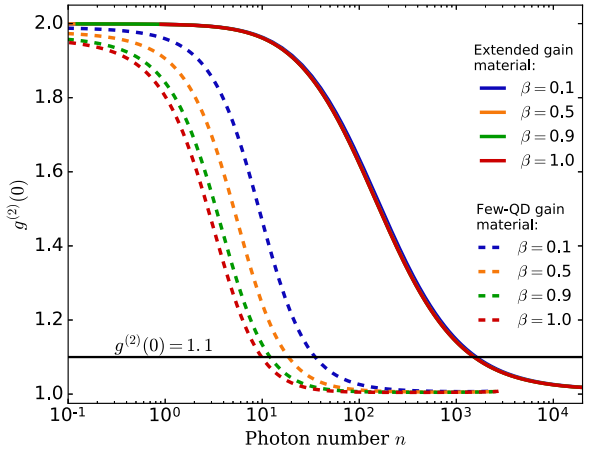

FIG. 4. Two-photon correlation function $g^{(2)}(0)$ as a function of photon number. For high-Q quantum-dot nanolasers (dashed lines) an increasing β factor leads to fewer photons required for coherent emission. For a high number of emitters and lower cavity Q (solid lines) coherent emission happens at much larger photon numbers and independent of β.

The only available $g^{(2)}(0)$ measurements performed in the parameter regime we associate with nanolasers with extended gain media are published in Ref. [26]. Upon close inspection, the results shown there indicate that the coherence threshold is also offset to the intensity threshold thereby confirming our prediction. At the same time, the results of our discrete-emitter model are in quantitative agreement with the semiconductor laser model used in the reference, which indeed supports the sufficiency of our approach. For the parameter regime of few-QD nanolasers, recent results have revealed mean photon numbers of $n \approx 100$ at the threshold without an offset between the intensity and coherence thresholds [41], which is exactly what is observed in Figs. 1 and 4 for a similar value of β.

The origin of the delayed formation of coherence and the insensitivity of the coherence threshold to the β factor can be understood from the contributions to the photon emission as expressed in Eq. (2b) assuming that coherence arises when stimulated emission dominates. Both stimulated emission $\propto n(2f - 1)$ and spontaneous emission $\propto f$ scale with the amount of gain material N. On the other hand, in the lasing regime the carrier population is close to f_L and the inversion $2f - 1$ is then approximately given by $2f_L - 1 = \kappa/(2RN)$ and, therefore, decreases with the number of emitters like $1/N$. Corrections to this approximation are provided by the right-hand side of Eq. (A11) in the Appendix, which is again of the order $1/N$. This is the reason why establishing coherence requires large photon numbers when N is large, and much lower n values in the few-emitter case, as demonstrated in Fig. 4. Technically, this behavior is also present in conventional lasers (such as gas and edge-emitting lasers) but is rendered irrelevant and goes unnoticed as the transition to coherent emission occurs sharply on a very narrow interval in such devices due to low β factors.

More insight is obtained from the analytical expression for the photon autocorrelation function. From Eq. (8) it is clear that as n becomes large, the first terms both in the numerator and the denominator become dominant and $g^{(2)}(0)$ approaches unity. Of course, the precise onset of coherence depends also on all parameters, but the dependence on β appears through Γ and R, which contain the sum of the loss rates $\gamma + \kappa$. Operating at higher cavity losses, the extended active medium system becomes insensitive to the rate of radiative loss. Two important conclusions are drawn from this observations. On the one hand, the benefits of high-β nanolasers in terms of $n = 1$ at threshold and low threshold pump powers due to increasing β rely on being close to the true few-emitter limit of nanolasing. On the other hand, in systems with many emitters or a large number of charge carriers in extended media, the influence of cavity losses on P_{coh} dominates that of radiative losses in device regimes relevant to high-β room-temperature lasing with 2D-gain media. Increasing

β in those regimes becomes less important than aiming for improved cavity design with higher quality factors Q.

IV. CONCLUSION

The prospect of strongly reducing the excitation power required to reach the threshold by minimizing radiative losses (i.e., $\beta \to 1$) is a key motivation in the development of nanolasers. By going beyond rate equations, we demonstrate that while this is indeed possible in operational regimes found in high-Q nanolasers with few emitters, novel devices based on extended gain media behave differently: There, coherence is established irrespective of the value of β. Having defined closed expressions for the laser intensity and coherence thresholds (the first indicating the intensity jump, the second the transition to coherent emission), we are able to identify that for the latter, the pump rate at which coherent emission is achieved is rather determined by the cavity losses and can only be improved by increasing Q rather than improving β. Our results stress the importance of statistical properties of the light emission, given by $g^{(2)}(0)$, and we provide an analytic expression that can be used in conjunction with rate-equation theories to access $g^{(2)}(0)$ to very good approximation. In the light of strong interest in novel ways to design nanolasers by means of new gain media and device geometries, our findings point to possible limitations of future nanolasers based on quantum-well and transition-metal dichalcogenide gain materials. More insight will be obtained once results on the statistical properties of such devices become available.

ACKNOWLEDGMENTS

The authors gratefully acknowledge funding by the DFG (Deutsche Forschungsgemeinschaft) and the DFG graduate school "Quantum Mechanical Materials Modelling QM^3". P.G. would like to thank the University of Bremen for their hospitality and the DFG for funding the visit. He acknowledges financial support from CNCS-UEFISCDI Grant No. PN-III-P4-ID-PCE-2016-0221.

APPENDIX A: DERIVATION OF THE RATE EQUATIONS

The system consists of N identical two-level emitters in resonance with a cavity mode. In the rotating frame, the Hamiltonian reads ($\hbar = 1$ throughout)

$$H = \sum_i [g b^\dagger v_i^\dagger c_i + g^* b c_i^\dagger v_i], \tag{A1}$$

with $b^\dagger, b$ operators for the photon mode, $c_i^\dagger, c_i$ for the upper (conduction-band) emitter states and $v_i^\dagger, v_i$ for the lower (valence-band) ones. We assume a single carrier per emitter, so that the c, v language is equivalent to the pseudospin formalism by $\sigma_i = v_i^\dagger c_i$ and $\sigma_i^\dagger = c_i^\dagger v_i$.

The equation of motion (EOM) for the expectation value of a given operator A contains, beside the coherent, von Neumann part, the dissipation expressed in the Lindblad form

$$\frac{d}{dt}\langle A\rangle = -i\langle [A,H]\rangle + \sum_\alpha \frac{\lambda_\alpha}{2}\langle [L_\alpha^\dagger, A]L_\alpha + L_\alpha^\dagger [A, L_\alpha]\rangle, \tag{A2}$$

where λ_α is the rate associated to the scattering process defined by the operator L_α. Three such processes are considered: the radiative loss in each emitter with λ_α denoted by γ and $L_\alpha = v_i^\dagger c_i$, the cavity losses with the rate κ and operator b, and the pumping simulated as an upscattering process, $L_\alpha = c_i^\dagger v_i$, with the rate P.

We apply Eq. (A2) to calculate the photon number $n = \langle b^\dagger b\rangle$ and the upper level population $f = \langle c_i^\dagger c_i\rangle$. Note that the latter does not depend on the emitter index i. One obtains

$$\frac{d}{dt} n = -\kappa n + 2N\,\mathrm{Re}\psi, \tag{A3}$$

$$\frac{d}{dt} f = -\gamma f + P(1-f) - 2\,\mathrm{Re}\psi. \tag{A4}$$

Both are expressed in terms of the real part of the photon-assisted polarization $\psi = -ig\langle b^\dagger v_i^\dagger c_i\rangle$. The EOM for ψ brings in higher-order expectation values, such as $\langle b^\dagger b c_i^\dagger c_i\rangle$. Such terms are treated in a mean-field approximation, which amounts to the truncation at the doublet level in the cluster expansion formalism [42,43]

$$\langle b^\dagger b c_i^\dagger c_i\rangle \approx \langle b^\dagger b\rangle\langle c_i^\dagger c_i\rangle = nf\,. \tag{A5}$$

The evolution of ψ also generates terms involving polarization operators $v^\dagger c, c^\dagger v$ from pairs of different emitters. They are discarded on reasons discussed in the next section. As a result one obtains

$$\frac{d}{dt}\psi = -\frac{\Gamma}{2}\psi + |g|^2 n(2f-1) + |g|^2 f\,, \tag{A6}$$

where $\Gamma = P + \gamma + \kappa$. This also shows that ψ is, in fact, a real quantity. The steady-state solution is identified by setting the time derivatives to zero. By eliminating ψ in the resulting equations one obtains for the populations

$$Rn(2f-1) + Rf = -\gamma f + P(1-f), \tag{A7a}$$

$$N[Rn(2f-1) + Rf] = \kappa n, \tag{A7b}$$

with the rate of spontaneous emission R given by

$$R = \frac{4|g|^2}{P+\gamma+\kappa}. \tag{A8}$$

The equations above are balance conditions. Their left-hand side contains the net photon generation rate, made up

of spontaneous and stimulated emission, as well as absorption. In Eq. (A7a) this is balanced against the rate of the emitter excitation, taking into account both the pumping and the radiative losses, while in Eq. (A7b) the photons generated by all emitters compensate the cavity losses.

Combining these equation one obtains

$$f_0 - f = \frac{\kappa n}{N(P+\gamma)}, \quad \text{with } f_0 = \frac{P}{P+\gamma}. \tag{A9}$$

It is obvious that f_0 is the steady-state upper-level population in the absence of the Jaynes-Cummings interaction ($R = 0$).

Equation (A7b) can be rewritten as

$$f_L - f = \frac{f}{2n}, \quad \text{with } f_L = \frac{\kappa}{2RN} + \frac{1}{2}, \tag{A10}$$

where f_L is the population for which the gain (stimulated emission minus absorption) exactly compensates the cavity losses. As seen from the above equations, one has $f \leqslant f_0, f_L$, i.e., both f_0 and f_L are upper bounds for the true steady-state solution. Multiplying Eqs. (A9) and (A10) one obtains a quadratic equation for f

$$(f_L - f)(f_0 - f) = \frac{\kappa f}{2(P+\gamma)N}, \tag{A11}$$

whose lower solution is the physical one. In turn, the photon population is given by

$$n = \frac{N(P+\gamma)}{\kappa}(f_0 - f). \tag{A12}$$

This solves the problem of steady-state populations for the carriers and for the photons at the rate-equation level.

In the limit $N \to \infty$ the rhs of Eq. (A11) vanishes and, as the pump increases, the solution changes abruptly from $f = f_0$ to $f = f_L$, always following the smaller. The $f = f_0$ case corresponds to pumping spent exclusively for exciting the carrier subsystem. This takes place until f reaches the value f_L with sufficient inversion to compensate the photon losses. From then on massive photon generation takes place, as seen in Eq. (A12), which shows the photon density $\eta = n/N$ changing sharply from $\eta = 0$ to $\eta \sim f_0 - f > 0$. This is the lasing regime (hence the index L), in which the photon number becomes macroscopic, i.e., scales like N. It becomes clear that in the limit $N \to \infty$ one obtains a sharp crossover from a "normal" regime to lasing. The threshold is defined by the pump value P_{th}, which obeys Eq. (5), expressing the crossing condition $f_0 = f_L$.

For finite values of N, the transition is no longer abrupt. The rhs of Eq. (A11) being nonzero, a smooth change (anticrossing) from $f \approx f_0$ to $f \approx f_L$ takes place. The lasing transition becomes gradual, without a well-defined threshold. Now a transition interval around P_{th} still separates two contrasting behaviors: Above it the photon number grows with system size N, while below it their number stays finite.

APPENDIX B: BEYOND RATE EQUATIONS: ACCESSING $G^{(2)}(0)$

The second-order autocorrelation function requires the cluster expansion at least up to the quadruplet level. This introduces a set of new expectation values besides the populations $n = \langle b^\dagger b\rangle$ and $f = \langle c_i^\dagger c_i\rangle$. The following notations are used below:

$$c_m = \langle b^{\dagger m} b^m c_i^\dagger c_i\rangle, \quad v_m = \langle b^{\dagger m} b^m v_i^\dagger v_i\rangle, \quad m = 0, 1, 2, \tag{B1}$$

$$p_m = \langle b^{\dagger m} b^m\rangle, \quad \psi_m = -ig\langle b^{\dagger m} b^{m-1} v_i^\dagger c_i\rangle, \quad m = 1, 2. \tag{B2}$$

With a single carrier in each emitter, these averages are not independent since, obviously $c_m + v_m = p_m$, but we keep the notation for convenience. Also, p_1 is the average photon number n, $c_0 = f$ and ψ_1 is the same as ψ of the previous section. The index i is spurious here, since all emitters are identical.

Quadruplet averages generated by equations of motion for doublet quantities are not factorized any more. As an example, consider the case of the one-photon-assisted polarization ψ_1, for a generic emitter i

$$\frac{d}{dt}\psi_1 = |g|^2(c_1 - v_1 + c_0) - \frac{1}{2}\Gamma\psi_1 + |g|^2 \sum_{j\neq i}\langle c_j^\dagger v_j v_i^\dagger c_i\rangle. \tag{B3}$$

In contrast to the rate equation, where one approximates $c_1 = p_1 c_0$, and $v_1 = p_1 v_0$, here we write new EOM for them. Having an additional $b^\dagger b$ factor in its definition, the evolution of c_1 generates the two-photon-assisted polarization ψ_2. The same holds for p_2, which is the central quantity of the two-photon autocorrelator $g^{(2)}(0)$. The equation for ψ_2 reads

$$\begin{aligned}\frac{d}{dt}\psi_2 = {} & |g|^2(c_2 - v_2 + 2c_1) - \frac{1}{2}\Gamma'\psi_2 \\ & + 2|g|^2 \sum_{j\neq i}\langle b^\dagger b c_j^\dagger v_j v_i^\dagger c_i\rangle \\ & - g^2 \sum_{j\neq i}\langle b^\dagger b^\dagger v_j^\dagger c_j v_i^\dagger c_i\rangle,\end{aligned} \tag{B4}$$

where $\Gamma' = P + \gamma + 3\kappa$. Quantities such as c_2 and v_2 are cluster expanded in terms of correlators as [42,43]

$$c_2 = \delta c_2 + \delta p_2 c_0 + 4\delta c_1 p_1 + 2p_1^2 c_0, \tag{B5}$$

and similarly for v_2. As a sixtuplet correlator, δc_2 is neglected, and using $\delta p_2 = p_2 - 2p_1^2$, $\delta c_1 = c_1 - p_1 c_0$, one obtains the expression of c_2 in its truncation at the quadruplet level as

$$c_2 = p_2 c_0 + 4 p_1 c_1 - 4 p_1^2 c_0. \tag{B6}$$

The summations appearing in both Eqs. (B3) and (B4) describe correlations of polarizations and photon-assisted polarization, respectively, between pairs of emitters. Bearing in mind that quantities on different sites are less correlated than same-site ones, we adopt the procedure of factorizing into averages on separate sites. For example,

$$\langle c_j^\dagger v_j v_i^\dagger c_i \rangle \approx \langle c_j^\dagger v_j \rangle \langle v_i^\dagger c_i \rangle. \tag{B7}$$

This expresses the sum in Eq. (B3) in terms of on-site polarizations. But these are anomalous averages, not driven by the system excitation, and as such are vanishing quantities. Therefore, this sum is taken as zero. This is not the case of the two sums in Eq. (B4), where by the same procedure we get $2(N-1)\psi_1\psi_1^*$ and $(N-1)\psi_1^2$, respectively. Since the equations obeyed by ψ_1 show that this is a real quantity, the two expressions are equal up to the prefactor, and a partial cancelation takes place, leaving the net result as $(N-1)\psi_1^2$. Let us emphasize that such terms, which express correlations between two emitters mediated by the photon field are usually neglected when one is not interested in superradiance effects [44]. In the present approach. they are included at a mean-field level.

The other EOM do not generate higher-order averages. As a result of the procedure described above, one is left with a closed system of EOM for $c_0, c_1, p_1, p_2, \psi_1$, and ψ_2. In the steady state, the time derivative vanishes and the system becomes algebraic. From this, one obtains an expression of p_2 and thus of $g^{(2)}(0)$ in terms of $c_0 = f$ and $p_1 = n$ only, by eliminating the other unknowns. The result is expressed in Eq. (6) of the main text. Further simplification arises by eliminating the upper-level population f in favor of the photon number n and inserting the rate-equation value of the latter, as described in the derivation of Eq. (8) of the main text. The approximation is very accurate, as shown in Fig. 5, which compares it to the result of using full quadruplet-computed populations in Eq. (6).

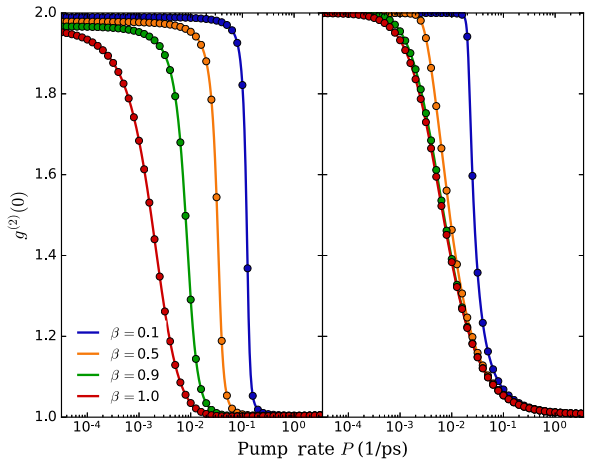

FIG. 5. Photon autocorrelation function $g^{(2)}(0)$ obtained by using full quadruplet (solid) and rate-equation (circles) populations. Both the few- (left) and many-emitter (right) cases are represented.

[1] H. Yokoyama and S. D. Brorson, Rate equation analysis of microcavity lasers, J. Appl. Phys. **66**, 4801 (1989).

[2] G. Björk and Y. Yamamoto, Analysis of semiconductor microcavity lasers using rate equations, IEEE J. Quantum Electron. **27**, 2386 (1991).

[3] W. W. Chow, F. Jahnke, and C. Gies, Emission properties of nanolasers during the transition to lasing, Light: Sci. Appl. **3**, e201 (2014).

[4] P. R. Rice and H. J. Carmichael, Photon statistics of a cavity-QED laser: A comment on the laser-phase-transition analogy, Phys. Rev. A **50**, 4318 (1994).

[5] P. Blood, The laser diode: 50 years on, IEEE J. Sel. Top. Quantum Electron. **19**, 1503201 (2013).

[6] Scrutinizing lasers, Nat. Photonics **11**, 139 (2017).

[7] Z. Wang, Z. Dong, Y. Gu, Y. Chang, L. Zhang, L. Li, W. Zhao, G. Eda, W. Zhang, G. Grinblat, S. A. Maier, J. K. W. Yang, C. Qiu, and A. T. S. Wee, Giant photoluminescence enhancement in tungsten-diselenide-gold plasmonic hybrid structures, Nat. Commun. **7**, 11283 (2016).

[8] S. Strauf and F. Jahnke, Single quantum dot nanolaser, Laser Photon. Rev. **5**, 607 (2011).

[9] P. Stepanov, A. Delga, N. Gregersen, E. Peinke, M. Munsch, J. Teissier, J. Mørk, M. Richard, J. Bleuse, J. M. Gérard, and J. Claudon, Highly directive and Gaussian far-field emission from "giant" photonic trumpets, Appl. Phys. Lett. **107**, 141106 (2015).

[10] D. G. Gevaux, A. J. Bennett, R. M. Stevenson, A. J. Shields, P. Atkinson, J. Griffiths, D. Anderson, G. a. C. Jones, and D. A. Ritchie, Enhancement and suppression of spontaneous emission by temperature tuning InAs quantum dots to photonic crystal cavities, Appl. Phys. Lett. **88**, 131101 (2006).

[11] M. Takiguchi, H. Sumikura, M. Danang Birowosuto, E. Kuramochi, T. Sato, K. Takeda, S. Matsuo, and M. Notomi, Enhanced and suppressed spontaneous emission from a buried heterostructure photonic crystal cavity, Appl. Phys. Lett. **103**, 091113 (2013).

[12] I. Prieto, J. M. Llorens, L. E. Muñoz Camúñez, A. G. Taboada, J. Canet-Ferrer, J. M. Ripalda, C. Robles, G. Muñoz Matutano, J. P. Martínez-Pastor, and P. A. Postigo, Near thresholdless laser operation at room temperature, Optica **2**, 66 (2015).

[13] Y. Ota, M. Kakuda, K. Watanabe, S. Iwamoto, and Y. Arakawa, Thresholdless quantum dot nanolaser, Opt. Express **25**, 19981 (2017).

[14] M. Khajavikhan, A. Simic, M. Katz, J. H. Lee, B. Slutsky, A. Mizrahi, V. Lomakin, and Y. Fainman, Thresholdless nanoscale coaxial lasers, Nature **482**, 204 (2012).

[15] S. Strauf, K. Hennessy, M. T. Rakher, Y.-S. Choi, A. Badolato, L. C. Andreani, E. L. Hu, P. M. Petroff, and D. Bouwmeester, Self-Tuned Quantum Dot Gain in Photonic Crystal Lasers, Phys. Rev. Lett. **96**, 127404 (2006).

[16] S. M. Ulrich, C. Gies, S. Ates, J. Wiersig, S. Reitzenstein, C. Hofmann, A. Löffler, A. Forchel, F. Jahnke, and P. Michler, Photon Statistics of Semiconductor Microcavity Lasers, Phys. Rev. Lett. **98**, 043906 (2007).

[17] M. Nomura, N. Kumagai, S. Iwamoto, Y. Ota, and Y. Arakawa, Laser oscillation in a strongly coupled single-quantum-dot-nanocavity system, Nat. Phys. **6**, 279 (2010).

[18] C. Gies, M. Florian, P. Gartner, and F. Jahnke, The single quantum dot-laser: Lasing and strong coupling in the high-excitation regime, Opt. Express **19**, 14370 (2011).

[19] P. Gartner and C. M. Halati, Laser transition in the thermodynamic limit for identical emitters in a cavity, Phys. Rev. A **93**, 013817 (2016).

[20] L. A. Coldren, S. W. Corzine, and M. L. Mashanovitch, *Diode Lasers and Photonic Integrated Circuits* (JohnWiley & Sons, Hoboken, New Jersey, 2012).

[21] F. Gericke, M. Segnon, M. von Helversen, C. Hopfmann, T. Heindel, C. Schneider, S. Höfling, M. Kamp, A. Musia, X. Porte, C. Gies, and S. Reitzenstein, Controlling the gain contribution of background emitters in few-quantum-dot microlasers, New J. Phys. **20**, 023036 (2018).

[22] S. Lichtmannecker, M. Florian, T. Reichert, M. Blauth, M. Bichler, F. Jahnke, J. J. Finley, C. Gies, and M. Kaniber, A few-emitter solid-state multi-exciton laser, Sci. Rep. **7**, 7420 (2017).

[23] N. Gregersen, T. Suhr, M. Lorke, and J. Mørk, Quantum-dot nano-cavity lasers with Purcell-enhanced stimulated emission, Appl. Phys. Lett. **100**, 131107 (2012).

[24] C. Gies, J. Wiersig, M. Lorke, and F. Jahnke, Semiconductor model for quantum-dot-based microcavity lasers, Phys. Rev. A **75**, 013803 (2007).

[25] P. Gartner, Two-level laser: Analytical results and the laser transition, Phys. Rev. A **84**, 053804 (2011).

[26] S. T. Jagsch, N. V. Triviño, F. Lohof, G. Callsen, S. Kalinowski, I. M. Rousseau, R. Barzel, J. Carlin, F. Jahnke, R. Butté, C. Gies, A. Hoffmann, N. Grandjean, and S. Reitzenstein, A quantum optical study of thresholdless lasing features in high-β nitride nanobeam cavities, Nat. Commun. **9**, 564 (2018).

[27] H. A. M. Leymann, C. Hopfmann, F. Albert, A. Foerster, M. Khanbekyan, C. Schneider, S. Höfling, A. Forchel, M. Kamp, J. Wiersig, and S. Reitzenstein, Intensity fluctuations in bimodal micropillar lasers enhanced by quantum-dot gain competition, Phys. Rev. A **87**, 053819 (2013).

[28] A. Carmele and A. Knorr, Analytical solution of the quantum-state tomography of the biexciton cascade in semiconductor quantum dots: Pure dephasing does not affect entanglement, Phys. Rev. B **84**, 075328 (2011).

[29] E. Schlottmann, M. von Helversen, H. A. M. Leymann, T. Lettau, F. Krüger, M. Schmidt, C. Schneider, M. Kamp, S. Höfling, J. Beyer, J. Wiersig, and S. Reitzenstein, Exploring the Photon-Number Distribution of Bimodal Microlasers with a Transition Edge Sensor, Phys. Rev. Appl. **9**, 064030 (2018).

[30] B. Calkins, P. L. Mennea, A. E. Lita, B. J. Metcalf, W. S. Kolthammer, A. Lamas-Linares, J. B. Spring, P. C. Humphreys, R. P. Mirin, J. C. Gates, P. G. R. Smith, I. A. Walmsley, T. Gerrits, and S. W. Nam, High quantum-efficiency photon-number-resolving detector for photonic on-chip information processing, Opt. Express **21**, 22657 (2013).

[31] R. Hanbury Brown and R. Q. Twiss, Correlation between photons in two coherent beams of light, Nature **177**, 27 (1956).

[32] H. Tian, M. L. Chin, S. Najmaei, Q. Guo, F. Xia, H. Wang, and M. Dubey, Optoelectronic devices based on two-dimensional transition metal dichalcogenides, Nano Res. **9**, 1543 (2016).

[33] Y. Li, J. Zhang, D. Huang, H. Sun, F. Fan, J. Feng, Z. Wang, and C. Z. Ning, Room-temperature continuous-wave lasing from monolayer molybdenum ditelluride integrated with a silicon nanobeam cavity, Nat. Nanotechnol. **12**, 987 (2017).

[34] O. Salehzadeh, M. Djavid, N. Tran, I. Shih, and Z. Mi, Optically pumped two-dimensional MoS2 lasers operating at room-temperature, Nano Lett. **15**, 5302 (2015).

[35] Y. Ye, Z. Wong, X. Lu, X. Ni, H. Zhu, X. Chen, Y. Wang, and X. Zhang, Monolayer excitonic laser, Nat. Photonics **9**, 733 (2015).

[36] S. Wu, S. Buckley, J. R. Schaibley, L. Feng, J. Yan, D. G. Mandrus, F. Hatami, W. Yao, J. Vucković, A. Majumdar, and X. Xu, Monolayer semiconductor nanocavity lasers with ultralow thresholds, Nature **520**, 69 (2015).

[37] A. Chernikov, C. Ruppert, H. M. Hill, A. F. Rigosi, and T. F. Heinz, Population inversion and giant bandgap renormalization in atomically thin WS_2 layers, Nat. Photonics **9**, 466 (2015).

[38] H. F. Hofmann and O. Hess, Quantum Maxwell-Bloch equations for spatially inhomogeneous semiconductor lasers, Phys. Rev. A **59**, 2342 (1999).

[39] W. W. Chow and M. H. Crawford, Analysis of lasers as a solution to efficiency droop in solid-state lighting, Appl. Phys. Lett. **107**, 141107 (2015).

[40] G. Björk, A. Karlsson, and Y. Yamamoto, Definition of a laser threshold, Phys. Rev. A **50**, 1675 (1994).

[41] S. Kreinberg, W. W. Chow, J. Wolters, C. Schneider, C. Gies, F. Jahnke, S. Höfling, M. Kamp, and S. Reitzenstein, Emission from quantum-dot high-β Transition from spontaneous emission to lasing and the effects of superradiant emitter coupling, Light: Sci. Appl. **6**, e17030 (2017).

[42] M. Kira and S. W. Koch, Semiconductor quantum optics (Cambridge University Press, Cambridge, New York, 2011).

[43] M. Florian, C. Gies, F. Jahnke, H. A. M. Leymann, and J. Wiersig, Equation-of-motion technique for finite-size quantum-dot systems: Cluster expansion method revisited, Phys. Rev. B **87**, 165306 (2013).

[44] H. A. M. Leymann, A. Foerster, F. Jahnke, J. Wiersig, and C. Gies, Sub- and Superradiance in Nanolasers, Phys. Rev. Appl. **4**, 044018 (2015).